RSC Advances

This is an *Accepted Manuscript*, which has been through the Royal Society of Chemistry peer review process and has been accepted for publication.

Accepted Manuscripts are published online shortly after acceptance, before technical editing, formatting and proof reading. Using this free service, authors can make their results available to the community, in citable form, before we publish the edited article. This *Accepted Manuscript* will be replaced by the edited, formatted and paginated article as soon as this is available.

You can find more information about *Accepted Manuscripts* in the Information for Authors.

Please note that technical editing may introduce minor changes to the text and/or graphics, which may alter content. The journal's standard Terms & Conditions and the Ethical guidelines still apply. In no event shall the Royal Society of Chemistry be held responsible for any errors or omissions in this *Accepted Manuscript* or any consequences arising from the use of any information it contains.

ROYAL SOCIETY OF CHEMISTRY

www.rsc.org/advances

Journal Name

RSCPublishing

ARTICLE

Optimisation of bi-layer resist overhang structure formation and SiO_2 sputter-deposition process for fabrication of gold multi-electrode array

Cite this: DOI: 10.1039/x0xx00000x

Received 00th January 2012, Accepted 00th January 2012

DOI: 10.1039/x0xx00000x

www.rsc.org/

Y. H. Kim,[a] G. H. Kim,[a] A.-Y. Kim,[a] N. S. Baek,[a] J. I. Jeong,[a] Y. H. Han,[a] B. C. Shin,[b] M.-A. Chung[a] and S.-D. Jung[a]

In this paper we report the results on the optimization of the bi-layer lift-off resist (LOR) SiO_2 sputter-deposition technique which is ideal for obtaining damage-free multi-electrode array (MEA). To optimize the bi-layer overhang formation, we have examined the undercut formation kinetics of LOR bottom layer and the dependence of the SiO_2 sputter-deposition lift-off processed electrode structure on the undercut length. Crater-shaped and recessed electrode structure is obtained when the undercut length is short (≤ 2 μm) and longer than 3 μm, respectively. To optimize the SiO_2 sputter-deposition process, we have examined the dependence of Au electrode passivation on the SiO_2 sputtering parameters in terms of electrochemical cyclic-voltammogram (C-V), impedance, electrical noise, sputter-deposition rate and *in vitro* neuronal activity recording property. The MEAs passivated under pure argon supply condition showed poor barrier properties, poor neuronal signal recording performance, and cytotoxic property. The C-V of MEAs passivated under oxygen mixing ratios above 5% showed traditional sigmoidal C-V and long-term recording of neuronal activities, probing the excellent barrier property and cytocompatibility of the SiO_2 films sputter-deposited under oxygen mixing conditions. We have also issued thermal damaging aspect of bi-layer overhang structure which is tightly coupled with the detailed electrode structure and the high sputter-deposition rate. Finally, it was suggested that measurement of C-V, electrochemical impedance and electrical noise can be a viable tool in evaluating the barrier performance of a passivation layer.

1 Introduction

Dielectric passivation of microelectrodes and interconnection lines is commonly applied in micro-fabricated devices, such as multi-electrode arrays (MEAs), biosensors, and neuroprobes, those are used in electrolyte solutions, to protect electrodes from degradation. Barrier property, mechanical stability, and corrosion resistance has been issued as an important factor determining the quality of passivation layer. Cytocompatibility, biocompatibility, and surface modification capability of the passivation layer are also regarded as an important factor when the devices are dealing with live cell, such as neuronal cell.

Many organic and inorganic materials have been used as passivation layer; SU-8,[1] photoresist (PR),[2] polydimethylsiloxane,[3] polyimide,[4] plasma-enhanced chemical vapour deposition (PECVD) silicon nitride (Si_3N_4)[5-6] and silicon oxide (SiO_2).[7,8] After intensive study on barrier and corrosion properties of PR, polyimide, PECVD SiO_2 and Si_3N_4, dual layers of SiO_2/Si_3N_4 and triple layers of $SiO_2/Si_3N_4/SiO_2$ based on PECVD SiO_2 and Si_3N_4, the triple layers had been experimentally demonstrated to yield long-term protection.[9] The multi-stack PECVD SiO_2 and Si_3N_4 films had been widely adopted in fabrication of silicon probes for simultaneous neural recording and drug delivery,[10] complementary metal-oxide-semiconductor MEA,[11] silicon-based neuroprobe,[12] and carbon nanotube MEA.[13] Recently, Temiz et al.[14] have addressed the quality and compatibility issues of passivation layer for microelectrodes in lab-on-a-chip applications through a comparative study on sputtered SiO_2, low pressure chemical vapor deposition (LPCVD) low-temperature oxide (LTO), parylene C, SU-8, and dry-film resist by means of impedance and electrochemical measurements. They reported that parylene C, SU-8, and LPCVD LTO show superior performance both in hydrolysis and impedance tests, and sputtered SiO_2 raises delamination issue. However, since they employed limited sputtering conditions there remain much to be optimized.

Very recently, we have introduced the bi-layer lift-off resist (LOR) sputter deposition as a new passivation technique useful for MEA fabrication.[15] Bi-layer consists of a photo-insensitive LOR sacrificing bottom layer and a negative PR patterning top layer, and has an overhang structure with undercut LOR layer. The bi-layer LOR sputter deposition technique is advantageous in that it does not require conventional reactive-ion etching (RIE) to open active electrode areas and uniform film thickness profile which is essential in RIE to avoid over etching, and that

RSC Advances Accepted Manuscript

This journal is © The Royal Society of Chemistry 2013

it provides electrodes without damages caused by reactive plasma. Even though the key unit processes, develop process to make overhang structure and RF sputter-deposition process to make dielectric films involved in the proposed technique are technically simple, there are lots of control parameters for each process. For instance, the quality of the sputter-deposited film is influenced by the oxygen content, working pressure, RF power, and so on. In this work we have examined the effect of the undercut forming and sputtering parameters on passivation performance in terms of electrochemical properties and *in vitro* neuronal activities recording capability.

2 Experimental

2.1 Formation of the bi-layer overhang structure

To form the bi-layer overhang structure, 3 μm thick photo-insensitive LOR (SF15, MicroChem) and 5 μm thick negative resist (AZ nLOF 2070, Clairant) film was subsequently spin-coated on the ITO substrate. After UV exposure through a Cr mask, the bi-layer was developed by AZ 300 MIF (Clairant) maintaining at 12 ± 0.1 °C (see S1, ESI†). Since, in the bi-layer LOR sputter-deposition technique, the diameter of the active electrode is determined by the bottom diameter of the LOR layer, the develop kinetics of the bi-layer was investigated by measuring the diameter of the LOR layer with respect to the develop time with optical microscopy. A test set of circular patterns having a diameter ranged from 10 to 40 μm was applied.

2.2 RF sputter-deposition of SiO_2

After forming the bi-layer overhang structure on the Au electrodes patterned by using standard photolithographic processes that are fully described in our previous report[15], RF sputter-deposition was carried out. High purity argon (99.999%) and oxygen (99.99%) were supplied through mass flow controllers after the base vacuum was reached to 5 x 10^{-6} Torr. The oxygen mixing ratio, defined as (oxygen feed rate) / (oxygen feed rate + argon feed rate), was varied from 0 % to 20 %. The high purity 3 inch SiO_2 target (99.9999%, Kojundo Chem Lab) loaded on a gun (Angstrom Science) was always pre-sputtered for 5 min to remove any contaminants on the target surface before deposition. The other sputtering parameters tuned in this study are as follows: RF (13.56 MHz) power (100 - 200 W), the sample-to-target distance (50 - 70 mm), and the substrate temperature (0 - 80 °C). While the fixed conditions are: argon feed rate of 50 sccm, working pressure of 4 mTorr, no sample rotation, and the ‘sputter up’ configuration. As a final step, lift-off of SiO_2 sputter-deposited overhang structure was conducted in LOR Remover PG (MicroChem) solution maintained at 60 °C with sonication for 30 min, followed by rinsing with running deionized water and drying with nitrogen gas.

2.3 Electrochemical characterisation

Prior to electrochemical characterization, a glass ring (internal diameter 21 mm, ring thickness 2 mm) was attached at the centre of the lift-off processed MEA with Sylgard 184 (Dow Corning). MEA was then exposed to oxygen plasma at 50W for 5min and stored in ethanol for 10 min. Electrochemical impedance spectroscopic (EIS) and C-V measurements were carried out using the ModuLab system (Solartron Analytical) with a three-electrode configuration: a fabricated Au MEA as a working electrode, a platinum plate as a counter electrode, and Ag/AgCl (sat’d KCl) as a reference electrode, respectively. The working electrode was connected to the analyser using a home-built pin-block which connects to each 60 channel Au electrode through contact pads. Prior to measurements, the Au electrodes were cleaned electrochemically by cycling the potential from -0.6 to 0.7 V (vs. Ag/AgCl, sat’d KCl) in 0.1M pH 7.2 PBS buffer. The electrochemical measurements were carried out in 0.1 M KCl solution containing 1.0 mM 1:1 $K_4Fe(CN)_6^{3-}$ /$K_3Fe(CN)_6^{4-}$. The EIS and C-V measurement was carried out in the range between 0.1 Hz and 100 kHz and at a scan rate 100 mV/s, respectively.

2.4 Primary neuronal cell culture and recording of neuronal activities

Primary neuronal cell cultures were performed with explants from embryonic day 17 Sprague–Dawley (SD) rat. Briefly, the cerebral cortex regions from embryonic day 17 SD rat fetuses were dissected in ice cold Ca^{2+}/Mg^{2+}-free Hanks’ balance salt solution (pH 7.4, Invitrogen). After removing the meninges, the cells were dissociated by trypsinization (0.25 % Trypsin - EDTA (1X), Invitrogen) followed by gentle blowing through an autoclaved pipette. The cell suspension was then plated at a cell density of 5×10^4 on MEA. Prior to cell plating, the glass ring attached MEA was exposed to oxygen plasma, followed by poly-D-lysine coating. Neurobasal culture medium (Invitrogen) was supplemented with a 2 % B27 supplement and 2.0 mM glutamin (Sigma), 10% FBS (Gibco) with antibiotics. The culture medium was replaced by fresh medium without FBS after 2 hrs and at every 3 days. The cells were grown and maintained at 37 °C and gas mixture (5 % CO_2 and 95 % humidified air) in a cell incubator (Thermo Scientific).

Neuronal signal measurement was performed with the home-constructed 60-channel recording system which characterized by a system ground noise of 2 μV. The neuronal activities were sampled at a rate of 20 kHz/channel, amplified (×1,200), and band-pass filtered (300-3,000 Hz). During the recording, the temperature was also maintained at 37.0 °C. In this study baseline noise root mean square level (V_{rms}), defined as $V_{rms} = (\Sigma V_k^2/K)^{1/2}$, where V_k (k = 1~ K) is extracted from the K = 3,000 (~1.5s) period in the recorded signal, was evaluated with and without neuronal cells.

3 Optimisation of the bi-layer overhang structure formation

Since the degree of undercut defines both the size of active electrode and the edge shape of the passivation layer, precise control of the LOR develop process is prerequisite in obtaining reproducible results. In general, slower rate is favoured in wet process for precise control. Fig. 1 (a) shows the typical dependence of diameter of the LOR layer on the develop time at 12 °C for different pattern diameter. The diameter of the LOR layer was determined from the top view optical microscope image taken with illumination from bottom side (see Fig. 1 (b)). We can find from Fig. 1 (a) that we can achieve the desired electrode diameter (e.g., 10 μm) from multiple pattern diameter larger than 10 μm or multiple electrode diameter (e.g., < 30 μm) from the 30 μm pattern simply by changing the develop time. Fig 1 (c) is a FESEM image confirming the formation of bi-layer overhang structure.

RSC Advances Accepted Manuscript

This journal is © The Royal Society of Chemistry 2012

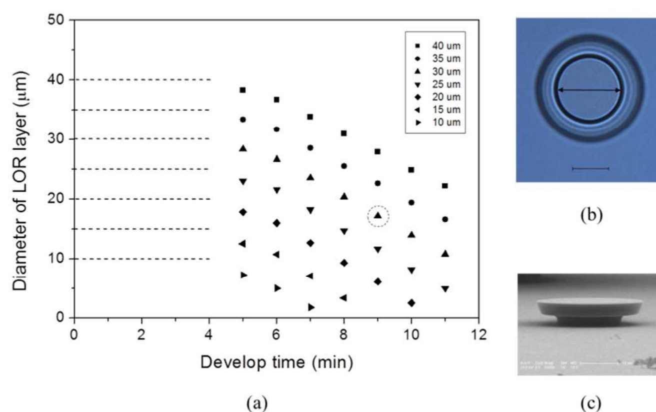

Fig. 1 (a) Develop kinetics of a LOR layer at 12 °C, (b) optical microscope image defining the diameter of the LOR layer, and (c) FESEM image representing the bi-layer overhang structure. The scale bars on (b) and (c) represent a length of 10 μm.

As shown in Fig. 2, sputter-deposition passivated electrodes show different structures depending on the undercut length. When the undercut length is short (< 1-2 μm), a crater-shaped electrode structure is obtained (Fig. 2 (a)). As the undercut length increases, recessed electrode structures are obtained (Fig. 2 (b) - (d)). The crater-shaped electrode structure is disadvantageous in that the crater wall might act as a fence for neurites approaching the electrode, resulting signal intensity decrease. Since we are particularly interested in recording of neuronal activities, in this study, we have focused on the MEAs having the recessed structure. To check quickly the electrochemical barrier performance of the recessed passivation structure, the bi-layer overhang structure was formed on the Au coated ITO substrate. After sputter-deposition and lift-off process, electro-deposition of Au nanoparticles (NPs) was carried out followed by sonication-treatment for 10 min form removal of dendrites. Fig. 2 (b), (c), and (d) shows clearly the Au NPs electro-deposited within the opened Au electrode,

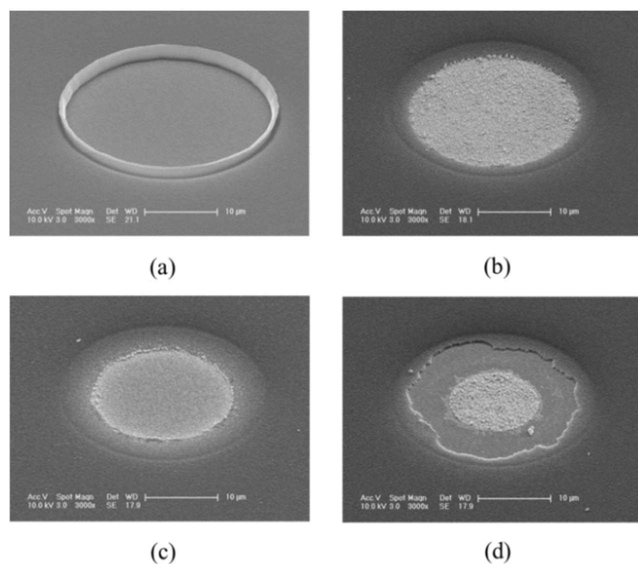

Fig. 2 FESEM images of electrodes lift-off processed with the bi-layer overhang structure having a various undercut length; (a) 2 μm, (b) 4 μm, (c) 5 μm and (d) 8 μm.

confirming that the recessed passivation film has sufficient electrochemical barrier resistance. However, when the undercut length is long (≥ *ca*. 8μm), the sputter-deposited SiO_2 film peeled off, as shown in Fig. 2 (d), after the sonication-treatment. This result is considered to be caused by the thin thickness of the passivation film and inherent poor adhesion strength between SiO_2 and Au. Thicker passivation films, rapid thermal annealing, and introduction of Cr or Ti as an adhesion promotion layer between SiO_2 and Au would protect peeling off.

Throughout these results, we have selected 3 - 6 μm as the optimal undercut length range in fabricating MEAs for *in vitro* extracellular recording of neuronal activities. Also we have adopted the 30 μm-sized mask pattern and fixed the develop time at 9 min, marked in Fig. 1 (a), so that overhang structures with bottom diameter of LOR layer of 18 ± 1 μm were repeatedly formed and used in optimisation of the SiO_2 sputter-deposition process.

4 Effect of sputtering parameters on passivation performance

4.1 Effect of oxygen mixing

Among barrier properties, electrical insulation or current leakage of passivation layer most strongly influences electrochemical properties of electrode. Since current leakage is caused by the pinholes, aqueous sorption process, and dielectric losses, their control is important. For example, dielectric loss of sputter-deposited film had already shown to be affected by the oxygen content.[16] Therefore we have investigated the effect of oxygen on the current leakage in terms of electrochemical C-V and impedance, electrical noise and neuronal activity recording capability. Fig. 3 shows the C-V of SiO_2 sputter-deposition passivated Au electrode with respect to the oxygen mixing ratio. When passivated under pure argon supply condition, the C-V resembles to the traditional one for large electrode exhibiting large currents and strong hysteresis, as shown in Fig. 3 (a), even though current peaks are not clearly seen. For comparison's sake C-V curve of the Au electrode sized 90 μm (solid line) is represented in Fig. 3 (a). Traditionally the strong hysteresis is caused by reduced contribution of diffusion compared with that of electron transfer. Since the electrode size does not change during the measurement the strong hysteresis would be contributed by the ITO interconnection lines in combination with porous nature of SiO_2 film sputter-deposited under pure argon supply condition. As the oxygen mixing ratio increases to 2.5%, the current density decreased to about $1 mAcm^{-2}$ and the measured C-V approaches to the sigmoidal one which reflects the matching of the rate of diffusion to the rate of electron transfer. We can observe the slight Ohmic contribution from the C-V of MEA passivated at oxygen mixing ratio of 2.5 %, and that, at oxygen mixing ratios above 5 %, the sigmoidal shape is almost independent of the oxygen mixing ratio.

Fig. 4 shows the electrical noise, sputter-deposition rate, and electrochemical impedance of electrode with respect to the oxygen mixing ratio. As shown in the figure, the electrical noise, electrochemical impedance, and deposition rate of the MEAs passivated under pure argon supply condition are quite different from those of the MEAs passivated with oxygen mixing. Conventionally, reduction in electrode impedance is resulted from surface area increase. However, since surface area of the active Au electrode unchanged during measurements

RSC Advances Accepted Manuscript

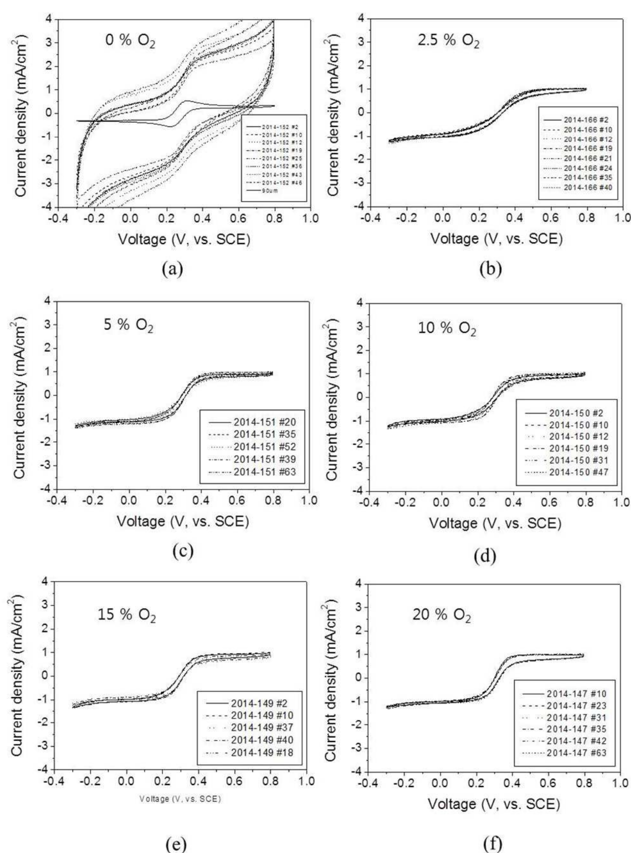

Fig. 3 C-V of SiO_2 sputter-deposition passivated Au MEA with respect to the oxygen mixing ratio. Sputtering conditions are; RF power of 150W and sample-to-target distance of 60mm.

and no surface modifications were performed to increase the surface area, the low impedance at pure argon supply condition is considered to be contributed by the ITO interconnection lines. It had been suggested that oxygen vacancies, formed at pure argon supply condition, may be involved in absorption of water or electrolyte via the formation of silanol groups ultimately resulting in dielectric losses.[17] Considering the relationship that the electrical noise is proportional to the square root of the impedance[18] the low electrical noise obtained under pure argon supply condition is attributed to the low impedance at that condition.

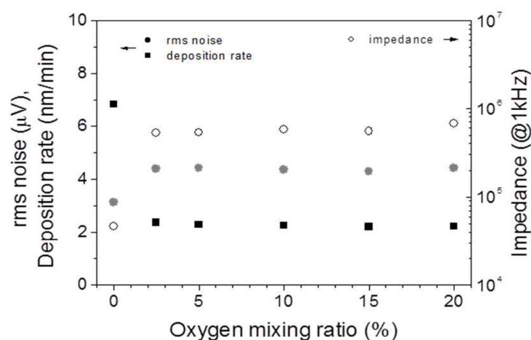

Fig. 4 Dependences of electrochemical impedance, electrical noise, and deposition rate on the oxygen mixing ratio. The data, except the deposition rate, were taken from 60 channels per MEA and averaged.

The deposition rate, which was determined from the cross-section FESEM image, is highest under pure argon supply condition and decreases rapidly upon supply of oxygen. The decrease in deposition rate upon oxygen supply had already been reported by several groups[16, 19-21] and had been explained in term of the replacement of sputtered oxygen atoms by oxygen from the gas phase before Si atom can be sputtered from the weakly bound state.[22, 23] Santamaria et al.[16] had also explained the effect of oxygen supply in terms of annihilation of defects consisting of oxygen vacancies. In our case, the sputter-deposition rate decreases rapidly upon supply of oxygen and saturates at above 5%, and this rapid decrease and saturation is close to that reported by Santamaria et al.[17] Some other groups[20, 24] reported gradual decrease even up to 45%, and we attribute this difference to the difference in sputter system used. To achieve uniform supply of gases we have placed a gas delivery unit with multiple nozzles close to target (see S2, ESI†). Although the pure argon supply condition resulted in the highest deposition rate, the low impedance indicates less sufficient barrier property emphasizing the importance of the oxygen mixing. The oxygen mixing is also already known to reduce the surface roughness, internal stress[21] and the grain size[20] and enhance the resistivity, breakdown field[25] and adhesion of the sputtered SiO_2 film to the glass.[20]

To see the effect of oxygen supply on neuronal activity recording performance of MEA, we have primarily cultured neuronal cell on the MEAs passivated with and without oxygen supply and recorded neuronal activities. Fig. 5 (a) shows the representative neuronal activities recorded at DIV 21 using MEA passivated at oxygen mixing ratio of 15%, and we could not find any significant differences in spike amplitude with respect to the oxygen mixing ratio except when pure argon is supplied. Maximum spike amplitude exceeding 150 μV indicates that Au MEAs passivated with SiO_2 sputter-deposition under oxygen mixing conditions have reasonable performance for neural spike recording. However, as shown in Fig. 5 (b), spike amplitude recorded at DIV 21 using MEA passivated under pure argon supply condition is lower (~50 μV), and only a few electrodes (3 - 5 electrodes) detected spikes. Even later at DIV 26 no spikes were detected. These results imply that the MEA passivated under pure argon supply

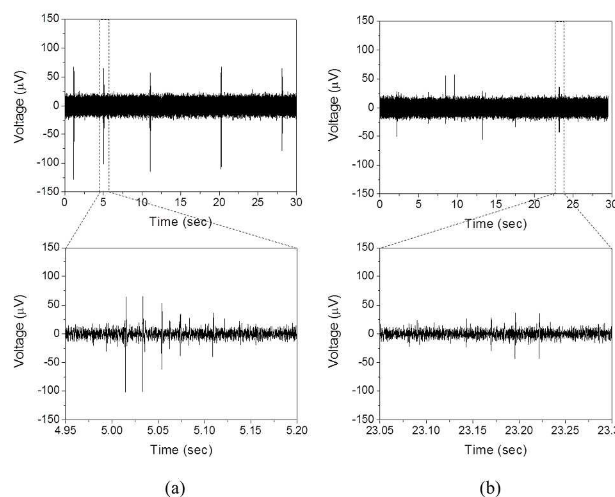

Fig. 5 Neuronal activities recorded at DIV 21 using (a) MEA passivated at oxygen mixing ratio of 15% and (b) MEA passivated under pure argon supply condition.

RSC Advances Accepted Manuscript

This journal is © The Royal Society of Chemistry 2012

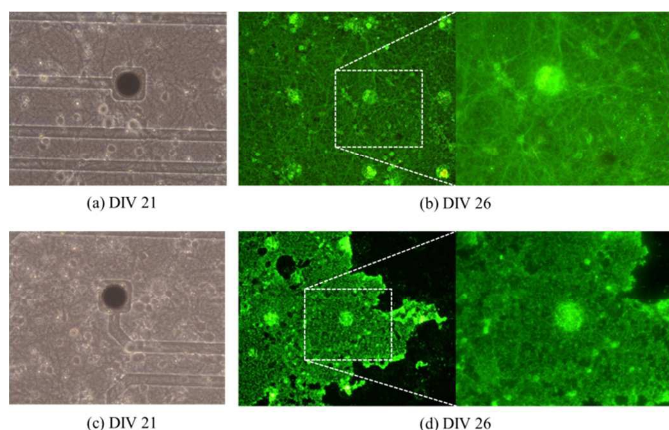

Fig. 6 Optical and fluorescence microscope image of neuronal cells primarily cultured on the MEA passivated (a) with (10%) and (b) without oxygen supply. The diameter of the circular Au patterns is 40 μm.

condition is not suitable for long-term *in vitro* neuronal recording, even though the condition yields the highest sputter-deposition rate under given other conditions.

To check the difference in recording performance of Au MEAs passivated with and without oxygen supply, we have observed the neuronal cells during (DIV 21) and after finishing the culture (DIV26). Fig. 6 (a) and (b) are the optical microscope image and the fluorescence microscope image, respectively, taken from MEA passivated with oxygen supply (oxygen mixing ratio of 10%) at DIV 21 (Fig. 6 (a)) and at DIV 26 (Fig. 6 (b)). Fig. 6 (c) and (d) were taken from MEA passivated without oxygen supply at DIV 21 (Fig. 6 (c)) and at DIV 26 (Fig. 6 (d)). For fluorescence microscopic identification, neuronal cells were stained with immunofluorescent anti-β-tublin (Covance) following the procedure described in our previous report.[34] We can find from the comparison of Fig. 6 (a) with (c) that neurites in Fig. 6 (c) are not as clear as those in Fig. 6 (a). This result indicates that the neuronal cells may form relatively less connections when they are cultured on MEA passivated without oxygen supply. This subtle difference at DIV 21 became clear at DIV 26. As shown in Fig. 6 (b), the neurites and cell bodies grown on MEA passivated with oxygen supply are lucid, while they are indistinguishable in Fig. 6 (d) which was taken from MEA passivated without oxygen supply. Since the Fig. 6 (d) shows the typical features of dead neuronal cells[26] it is deduced that the MEA passivated under pure argon condition has poor neuronal cell viability, and is even toxic to neuronal cells.

4.2 Substrate temperature effect and thermal damaging aspect

Substrate heating during the sputter-deposition is advantageous in increasing film adhesive strength, density, and resistivity, decreasing overall surface roughness,[27] and eliminating pinholes via reduction of H_2O.[28] However, in this work, the substrate heating is limited by glass temperature (*ca*. 190 °C) of SF15 LOR layer and thermally induced deformation of cross-linked top layer. It had been reported that, without heating, the substrate temperature increased from room temperature to 160 °C during the sputtering at RF power of 200 W.[29] Considering this plasma-induced substrate temperature increment, we have observed effect of substrate temperature on passivation performance in terms of C-V characteristics within a temperature range between 0 to 80 °C at RF power of 150 W. However, we could not find any remarkable differences in C-V with respect to substrate temperature within the applied range. We are routinely maintaining the temperature of substrate holding stage at 60 °C just to protect the MEA from water absorption. It had been demonstrated that rapid thermal annealing (RTA) improves the dielectric property of the oxygen-argon sputter-deposited SiO_2 comparable to thermal oxide.[32,33] Since the as-passivated MEAs showed enough barrier property during electro-deposition of metal nanoparticles and long-term neuronal recording capability up to three months, we did not perform any extra thermal treatment. RTA would be effective in which qualitative measurement of signal intensity is important, such as electrochemical bio-sensing.

In view of throughput, the higher deposition rate is favoured because it can save process time, unless it does not accompany negative effects. Review of the previous reports summarized that the deposition rate is utmost sensitive to RF power and sample-to-target distance.[20,29-31] Therefore, we have investigated the effect of the RF power and the sample-to-target distance on the deposition rate for our sputter system, and found that deposition rate can be increased by 1 nm/min by decreasing sample-to-target distance from 60 mm to 50 mm or by increasing RF power from 150 W to 200 W, respectively (see S3, ESI†). However, the sample-to-target distance decrease and the RF power increase are inevitably accompanied by substrate temperature increase, so that deformation of bi-layer overhang structure is expected. Fig. 7 (a) shows the cross-section FESEM image of the SiO_2 sputter-deposited bi-layer overhang structure at sample-to-target distance of 50 mm and 200 W RF power. As expected, we could observe the bent overhang structure hampering the film formation underneath the overhang structure. The depth profile of the recessed electrode obtained from atomic force microscope (AFM) image, as shown in Fig. 7 (b), confirms the influence of the bent overhang structure by exhibiting reduced film thickness as indicated by an arrow. The application of thicker and mechanically more rigid top patterning layer would enable to achieve the higher sputter-deposition rate and much more robust passivation. Also the introduction of metal film as a sacrificing bottom layer would make it possible to perform sputter-deposition at substrate temperatures higher than 200 °C, resulting in the high quality passivation film comparable to thermal oxides.

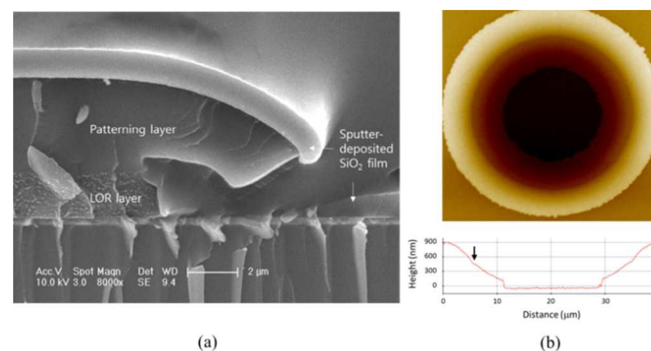

Fig. 7 (a) FESEM image of the cross-section of the SiO_2 sputter-deposited bi-layer overhang structure at RF power of 200 W and sample-to-target distance of 40 mm and (b) AFM image of the lift-off processed electrode.

RSC Advances Accepted Manuscript

Conclusions

We have examined the undercut formation kinetics of bi-layer (negative PR top layer and LOR bottom layer) overhang structure and the dependence of SiO_2 sputter-deposition lift-off processed electrode structure on the undercut length. Crater-shaped and recessed electrode structure is obtained when the undercut length is short (≤ 2 μm) and longer than 3 μm, respectively. We have selected 3 - 6 μm as the optimal undercut length range in fabricating MEAs for *in vitro* extracellular recording of neuronal signals. We have also examined the dependence of MEA passivation on the SiO_2 sputtering parameters in terms of electrochemical C-V, impedance, electrical noise, sputter-deposition rate and *in vitro* neuronal activity recording property. It was found that MEA passivation is sensitive to the oxygen supply and insensitive to the substrate temperature within the range between 0 and 80 °C. The MEAs passivated under pure argon supply condition showed poor barrier property, poor neuronal signal recording performance, and poor cytocompatibility probably due to oxygen vacancies. The MEAs passivated at oxygen mixing ratios higher than 5 % showed ideal sigmoidal C-V, confirming the reasonable barrier property of the sputter-deposited SiO_2 films. In this study, the simple bi-layer LOR sputter-deposition technique is proved to provide not only the robust passivation without delamination but also damage-free metal electrode which is useful as a platform in constructing highly sensitive and reproducible sensor on a chip.

It is noteworthy that as described in our previous reports[15] the SiO_2 sputter-deposition lift-off processed Au electrodes have the capability to be surface-modified with metal nanoparticles via the electro-deposition, leading to the reduction in noise level. Electro-co-deposition of various pairs of metals is under performing and the detailed results will be reported to elsewhere.

Acknowledgements

This study was supported by the Pioneer Research Centre Program through National Research Foundation of Korea funded by the Ministry of Science, ICT & Future Planning (2012-0009464) and by Electronics & Telecommunications Research Institute (project 14ZE1160).

Notes and references

[a] Electronics and Telecommunications Research Institute, Synapse Device Creative Research Centre, 218 Gajeong-ro, Yuseong-gu, Daejeon, 305-700, South Korea. Email: jungpol@etri.re.kr; Tel: +82 42 860 5557.

[b] Pusan National University, Department of Rehabilitation Medicine, Yangsan, 626-870, South Korea. E-mail: drshinbc@pusan.ac.kr; Fax: +82 51 510 8420; Tel: +82 55 360 5945.

† Electronic Supplementary Information (ESI) available: Photos of the experimental setup for precise develop temperature control, photos of the gas delivery unit mounted on the sputter gun for uniform supply, and dependence of the deposition rate on RF power and sample-to-target distance for sputter system. See DOI: 10.1039/b000000x/

1 E. Seker, Y. Berdichevsky, M. R. Begley, M. L. Reed, K. J. Stanley and M. L. Yarmush, *Nanotechnol.*, 2010, **21**, 125504.

2 R. D. Gardner, A. Zhou and N. A. Zufelt, *Sens. Actuators B Chem.*, 2009, **136**, 177-196.

3 L. Guo, K. W. Meacham, S. Hochman and S. P. DeWeerth, *IEEE Trans. Biomed. Eng.*, 2010, **57**, 2485-2494.

4 S.-P. Lin, J. J. Chen, J.-D. Liao and S.-F. Tzeng, *Biomed. Microdevices*, 2008, **10**, 99-111.

5 U. Egert, B. Schlosshauer, S. Fennrich, W. Nisch, M. Fejtl, T. Knott, T. Müller and H. Hämmerle, *Brain Res. Protoc.*, 1998, **2**, 229-242.

6 J.-H. Kim, G. Kang, Y. Nam and Y.-K. Choi, *Nanotechnol.*, 2010, **21**, 085303.

7 K. M. Wassum, V. M. Tolosa, J. Wang, E. Walker, H. G. Monbouquette and N. T. Maidment, *Sensors*, 2008, **8**, 5023-5036.

8 G. I. Mijares, D. R. Reyes, J. Geist, M. Gaitan, B. J. Polk and D. L. DeVoe, *J. Res. Natl. Inst. Stand. Technol.*, 2010, **115**, 61-73.

9 G. Schmitt, J. W. Schultze, F. Faβbender, G. Buβ, H. Luth and M. J. Schöning, *Electrochim. Acta*, 1999, **44**, 3865-3883.

10 K. Seidl, S. Spieth, S. Herwik, J. Steigert, R. Zengerle, O. Paul and P. Ruther, *J. Micromech. Microeng.*, 2010, **20**, 105006.

11 F. Heer, W. Framks, A. Blau, S. Taschini, C. Ziegler, A. Hierlemann and H. Baltes, *Biosens. Bioelectron.*, 2004, **20**, 358-366.

12 H. Zhao, W. H. Pei, S. Y. Chen, Q. Gui, R. Y. Tang, K. Guo and H. D. Chen, *Sci. China Tech. Sci.*, 2012, **55**, 2436-2440.

13 K. Wang, H. A. Fishman, H. Dai and J. S. Harris, *Nano Lett.*, 2006, **6**, 2043-2048.

14 Y. Temiz, A. Ferretti, Y. Leblebici and C. Guiducci, *Lab Chip*, 2012, **12**, 4920-4928.

15 Y. H. Kim, G. H. Kim, N. S. Baek, Y. H. Han, A.-Y. Kim, M.-A. Chung and S.-D Jung, *J. Micromech. Microeng.*, 2013, **23**, 097001.

16 J. Santamaria, E. Iborra, F. S. Quesada, G. G. Diaz and M. R. Vidal, *Thin Solid Films*, 1986, **139**, 201-208.

17 J. Santamaria, F. S. Quesada, G. Diaz, E. Iborra and M. R. Vidal, *Thin Solid Films*, 1985, **125**, 299-303.

18 J. E. Ferguson, C. Boldt and A. D. Redish, *Sens. Actuators A*, 2009, **156**, 338-393.

19 H. Jacobsson and G. Holmen, *Nucl. Instrum. Methods Phys. Res. B*, 1993, **82**, 291-300.

20 W.-F. Wu and B.-S. Chiou, *Appl. Surf. Sci.*, 1996, **99**, 237-243.

21 H. Fujiyama, T. Sumomogi and T. Endo, *J. Vac. Sci. Technol. A*, 2002, **20**, 356-361.

22 M. Cantagrel and M. Marchal, *J. Mater. Sci.*, 1973, **8**, 1711-1716.

23 E. H. Hasseltine, F. C. Hurlbut, N. T. Olson and H. P. Smith Jr., *J. Appl. Phys.*, 1967, **38**, 4313-4316.

24 Z. Xuping, L. Qing and Z. Haokang, *J. Electron. Mater.*, 1988, **27**, 1347-1350.

25 S. Suyama, A. Okamoto and T. Serikawa, *J. Electrochem. Soc.: Solid-State Sci. Technol.*, 1987, **134**, 2260-2264.

26 R. M. R. Pizzi, D. Rossetti, G. Cino, D. Marino, A. L. Vescovi and W. Baer, *BioSystems*, 2009, **95**, 137-144.

27 J. Ma, F. Ran, M. Xu and H. Ji, *J. Semicond.*, 2011, **32**, 044002.

28 H. Nagata, T. Fujino, N. Mitsugi and M. Tamai, *Thin Solid Films*, 1998, **335**, 117-121.

29 V. Bhatt and S. Chandra, *J. Micromech. Microeng.*, 2007, **17**, 1066-1077.

30 W.-F. Wu and B.-S. Chiou, *Thin Solid Films*, 1994, **247**, 201-207.

31 D. J. Kang, J. S. Kim, S. W. Jeong, Y. Roh, S. H. Jeong and J. H. Boo, *Thin Solid Films*, 2005, **475**, 160-165.

32 W. K. Choi, C. K. Choo and Y. F. Lu, *J. Appl. Phys.*, 1996, **80**, 5837-5842.

RSC Advances Accepted Manuscript

 This journal is © The Royal Society of Chemistry 2012

33 G. Eftekhari, *Phys. Stat. Sol. (a)*, 1995, **151**, 129-133.
34 Y. H. Kim, N. S. Baek, Y. H. Han, M.-A. Chung and S.-D. Jung, *J. Neurosci. Methods*, 2011, **202**, 38-44.

RSC Advances Accepted Manuscript

This journal is © The Royal Society of Chemistry 2012